



TITLE:

Thermotropic liquid crystalline properties of (hydroxypropyl)cellulose derivatives with butyryl and heptafluorobutyryl substituents

AUTHOR(S):

Ishii, Hirokazu; Sugimura, Kazuki; Nishio, Yoshiyuki

CITATION:

Ishii, Hirokazu ...[et al]. Thermotropic liquid crystalline properties of (hydroxypropyl)cellulose derivatives with butyryl and heptafluorobutyryl substituents. Cellulose 2018, 26(1): 399-412

ISSUE DATE:

2018-01

URL:

<http://hdl.handle.net/2433/241087>

RIGHT:

This is a post-peer-review, pre-copyedit version of an article published in 'Cellulose'. The final authenticated version is available online at: <https://doi.org/10.1007/s10570-018-2176-6>; The full-text file will be made open to the public on 08 December 2019 in accordance with publisher's 'Terms and Conditions for Self-Archiving'; この論文は出版社版ではありません。引用の際には出版社版をご確認ください。; This is not the published version. Please cite only the published version.

1

2 **Thermotropic liquid crystalline properties of (hydroxypropyl)cellulose derivatives with**
3 **butyryl and heptafluorobutyryl substituents**

4

5

6

7 Hirokazu Ishii, Kazuki Sugimura*, Yoshiyuki Nishio

8

9 *Division of Forest and Biomaterials Science, Graduate School of Agriculture, Kyoto*

10 *University, Sakyo-ku, Kyoto 606-8502, Japan*

11

12 *Corresponding author. Phone: +81 75 753 6252

13 E-mail address: kazusugi@kais.kyoto-u.ac.jp (K. Sugimura)

14

Abstract: (Hydroxypropyl)cellulose (HPC) derivatives with butyryl (Bu) and heptafluorobutyryl (7FBu) substituents were prepared in various proportions of the Bu/7FBu groups and at a fixed total DS ($DS_{\text{Bu}} + DS_{7\text{FBu}}$) of 3.0. Thermotropic liquid crystallinity of the derivatives (Bu7FBu-HPC) was investigated to specify the effect of the fluoroacylation on the mesophase behavior. Thermal transition data were collected using differential scanning calorimetry and polarized light microscopy. The Bu7FBu-HPC samples formed a chiral nematic phase between their glass transition and isotropization temperatures, T_g and T_{i-a} , respectively; these transition temperatures rose moderately as the 7FBu proportion increased ($T_g = -44$ – -27 °C and $T_{i-a} = 158$ – 190 °C for $DS_{7\text{FBu}} = 0.04$ – 1.60). The structural property of the mesophase was examined at 70 °C by circular dichroism and other optical measurements. The chiral nematic pitch (P) sensitively increased with increasing 7FBu proportion, while the supramolecular helical arrangement remained right-handed. Selective light-reflection colors were observed for the samples of $DS_{7\text{FBu}} = 0.04$ – 0.8 , covering an entire spectrum range from violet to red. Temperature dependence of P was also examined for selected samples below T_{i-a} , and it was found to increase with increasing temperature; however, there was no indication of inversion in the handedness of the helical structure. Wide-angle X-ray diffractometry revealed that the increases of P responding to the increases in $DS_{7\text{FBu}}$ and temperature were attributable to the decrease of the twist angle between adjacent thin nematic layers.

Keywords: (Hydroxypropyl)cellulose (HPC); HPC ester; Fluoroacylation; Thermotropic liquid crystal; Chiral nematic structure

Introduction

Cellulosic polymers can form a liquid crystalline phase in a condensed fluid state because of the inherent semirigidity in the carbohydrate backbone (Fukuda et al. 1994; Fukuda et al. 1995; Gray 1994; Gray and Harkness 1994; Guo and Gray 1994; Nishio et al. 2016; Zugenmaier 1994; Zugenmaier 1998). The supramolecular arrangement in the mesophase is mostly chiral nematic (synonymous with cholesteric), probably originating from a chiral nature (asymmetry) in the molecular structure. (Hydroxypropyl)cellulose (HPC) is a familiar liquid-crystalline cellulose derivative and offers the chiral nematics in a variety of common solvents (Gilbert and Patton 1983; Gray 1983, 1985, 1994; Guo and Gray 1994; Nishio 2006; Nishio et al. 2016; Zugenmaier 1998). This type of mesophase often imparts a vivid color due to selective light reflection, when the supramolecular helical periodicity (i.e., pitch P) is comparable to wavelengths of visible light. For instance, HPC solutions in water exhibit such a typical optical character at polymer concentrations of ca. 50–70 wt% (Werbowskyj and Gray 1976, 1980). With regard to thermotropic liquid crystals realized in melt without any solvents, several derivatives of HPC obtained by esterifying or etherifying the hydroxyl groups of HPC were reported to form stable chiral nematic phases that displayed iridescent colors over a range of temperatures (Guittard et al. 1994; Hou et al. 2000; Huang et al. 2007; Ishizaki et al. 2015; Kosho et al. 1999; Ohlendorf and Greiner 2015; Ritcey and Gray 1988; Tseng et al. 1981; Yamagishi et al. 1994; Yamagishi et al. 2006). Those HPC ester/ether series can serve as media for a thermal sensor, or a display or light reflection device adaptable to various temperature conditions.

For the thermotropics of alkyl esters (normal acylates) of HPC (Hou et al. 2000; Huang et al. 2007; Kosho et al. 1999; Yamagishi et al. 1994), we find the following general tendencies regarding the chiral nematic pitch P : (1) As the alkyl chain-length increases, the thermal range involving mesophase formation shifts downwards and the pitch P increases at a

constant temperature; (2) P decreases with increasing degree of substitution (DS) for the acyl group; (3) the handedness of the supramolecular helical arrangement is always right-handed. Concerning the temperature dependence of P , it appears certain that P increases with temperature unless the carbon number (n) of the introduced acyl group exceeds at least 5 (Kosho et al. 1999; Yamagishi et al. 1994); however, there is a claim to have discovered the negative dependence of P on temperature for the HPC esters with $n = 7-9$ (Kosho et al. 1999).

A few reports dealt with thermotropic behavior of HPC esters containing fluorocarbon components, such as a fully substituted perfluorooctanoate of HPC (Guittard et al. 1994; Yamagishi et al. 1994). For example, it was inferred that the reverse pitch (P^{-1}) of the fluoroacylated derivatives would be larger (i.e., the P would be smaller) than that of HPC esters with the corresponding hydrocarbon substituents, when compared at the same temperature (Yamagishi et al. 1994). However, the actual comparison was not made based on quantitative P data between the two sorts of HPC derivatives having the same number of carbons in the substituents, and therefore that conclusion seems to be rough-and-ready.

In the present study, we prepared a kind of mixed ester of HPC with two different acyl substituents of $n = 4$, butyryl (Bu) and heptafluorobutyryl (7FBu) substituents, at the total DS = 3 and in various proportions of the 7FBu to Bu groups. The reason for the selection of the carbon number $n = 4$ was that butyrylated HPC (Bu-HPC) had been well characterized for the thermotropy and reported to exhibit reflective colorations in a wide temperature range of ca. 20–90 °C (Hou et al. 2000; Huang et al. 2007; Yamagishi et al. 1994); the range is convenient in practice. The objective of this paper is to clarify the effect of fluoroacylation on the chiral nematic properties of the thermotropic HPC derivative (termed Bu7FBu-HPC). It is shown that the 7FBu introduction, even at quite a low DS_{7FBu} of <0.15, drastically "increases" the chiral nematic pitch.

Experimental

Materials

The HPC used was a commercially available powder sample (Scientific Polymer Products, Inc., lot no. 491018005); the nominal molecular weight was 60,000. On the basis of GPC measurements (see below), the number-average and weight-average molecular weights of this HPC were estimated as $M_n = 2.02 \times 10^4$ and $M_w = 7.29 \times 10^4$, respectively. The degree of side-group substitution was evaluated as $DS_{pr} = 2.93$ and $MS_{pr} = 4.87$ from 1H and ^{13}C NMR measurements (Ho et al. 1972; Lee and Perlin 1982), where DS_{pr} and MS_{pr} denote an average number of substituted hydroxyls and that of introduced hydroxypropyl groups, respectively, per anhydroglucose unit (AGU).

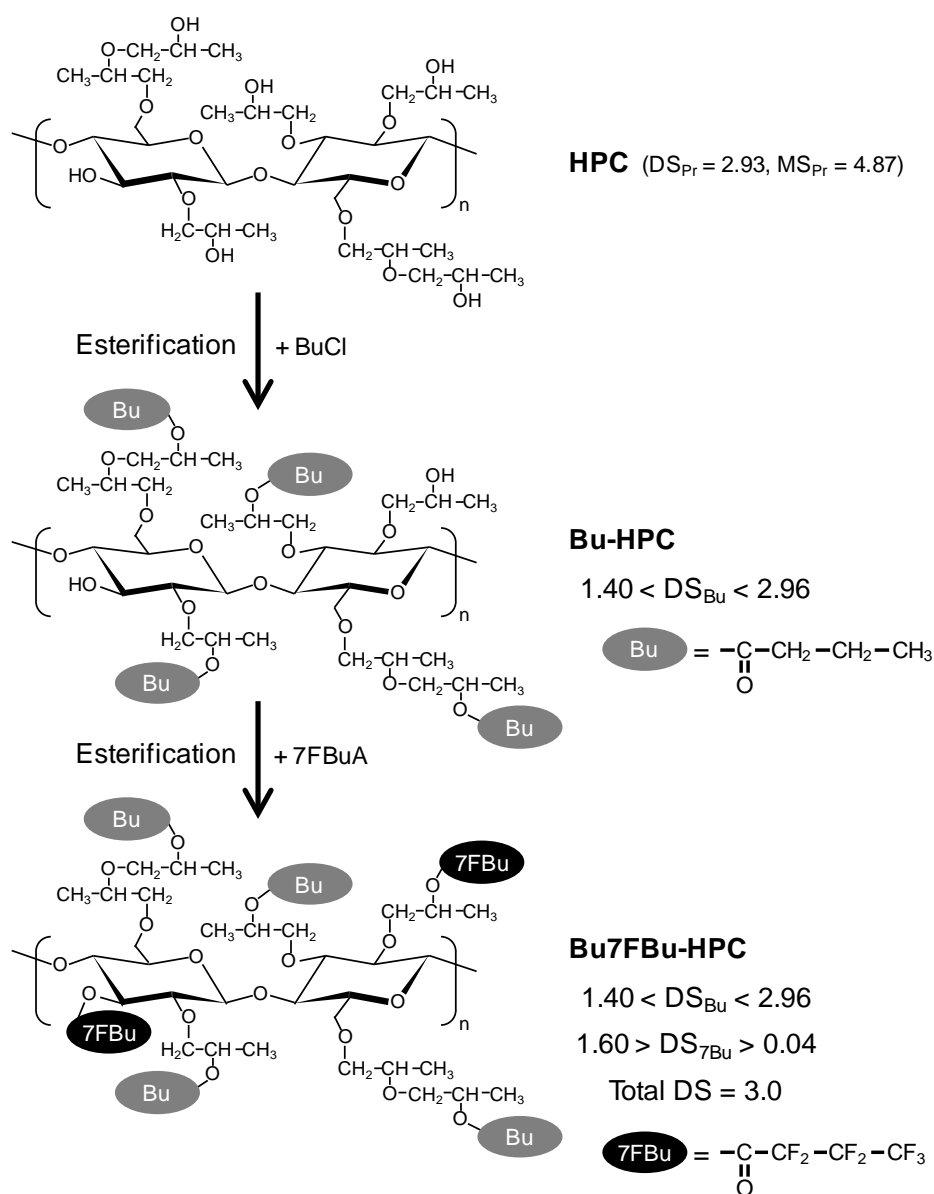
Butyryl chloride (BuCl), pyridine (dehydrated), and tetrahydrofuran (THF; containing no stabilizer) were purchased from Wako Pure Chemical Industries. Heptafluorobutyric acid anhydride (7FBuA) was purchased from Sigma-Aldrich, and acetone and other reagents were products of Nacalai Tesque, Inc. All the chemicals were guaranteed reagent-grade and used as received.

Synthesis of Bu7FBu-HPC

Synthesis of the objective derivative Bu7FBu-HPC was conducted via a two-step pathway of reaction (Scheme 1); HPC was first butyrylated with BuCl and then the residual OH groups of the product Bu-HPC were esterified with 7FBuA. In the first step, typically 5.0-g HPC (dried powder) was completely dissolved in 70-mL THF at room temperature (20 °C) and the prescribed amount of pyridine (4.0–18 eq/AGU) as a basic catalyst was added into the solution. After heating the solution to 40 °C, BuCl was added thereto. The

117 butyrylation of HPC with BuCl was carried out in various conditions of the attacking reagent
118 amount and reaction time, as shown in Table 1, but at a constant temperature of 40 °C under a
119 nitrogen atmosphere. In the termination of the reaction, the solution was poured into an
120 excess amount of distilled water and the precipitate Bu-HPC was collected by filtration. The
121 crude Bu-HPC was purified by dissolution–reprecipitation with acetone and distilled water.
122 The purified Bu-HPC was dried under vacuum at 40 °C for 24 h. We prepared ten Bu-HPC
123 samples listed in Table 1.

124



125

126 **Scheme 1** Synthetic pathway to Bu7FBu-HPC from HPC

127

128 **Table 1** Reaction conditions for preparation of Bu-HPC (at 40 °C)

Sample code	HPC (g)	THF (mL)	Time (h)	Pyridine in feed*	BuCl in feed*
Bu _{2.96} -HPC	3.0	40	5.0	18	9.0
Bu _{2.95} -HPC	3.0	40	2.5	18	9.0
Bu _{2.92} -HPC	5.0	70	1.0	18	9.0
Bu _{2.87} -HPC	5.0	70	0.50	18	9.0
Bu _{2.86} -HPC	5.0	70	0.25	18	9.0
Bu _{2.67} -HPC	5.0	70	0.50	9.0	4.5
Bu _{2.56} -HPC	5.0	70	0.50	7.5	3.8
Bu _{2.23} -HPC	5.0	70	0.50	6.8	3.4
Bu _{2.11} -HPC	5.0	70	0.50	6.0	3.0
Bu _{1.40} -HPC	5.0	70	0.50	4.0	2.0

* Represented by the molar ratio to an AGU of HPC.

129

130 Next, the Bu-HPC samples were each further esterified with 7FBuA in a similar
131 procedure, but using the same reaction conditions: Bu-HPC reactant, 1.5 g; THF solvent, 25
132 mL; pyridine, 18 eq/AGU; 7FBuA, 9.0 eq/AGU; reaction time, 24 h; reaction temperature,
133 40 °C. Each purified product is encoded as Bu_x7FBu_y-HPC (see Table 2), where $x = DS_{Bu}$
134 and $y = DS_{7FBu}$, i.e., DSs for the two substituents, and actually it was derived from Bu_x-HPC
135 of the corresponding sample code in Table 1.

136

137 Measurements

138

139 ¹H NMR spectra were acquired using a Varian NMR system 500 MHz with an oneNMR
140 5MM probe in the following conditions: solvent, CDCl₃; temperature, 23 °C; solute
141 concentration, 10 mg/0.7 mL; internal standard, tetramethylsilane (TMS); recycle time, 8.5 s;
142 number of scan, 32. FT-IR spectra were acquired using a Shimadzu IRPrestige-21
143 spectrometer. A pellet of pristine KBr was first made and then a few drops of polymer

solution (1 wt% Bu7FBu-HPC in chloroform) were dropped onto the pellet. The wet pellet was vacuum dried at 40 °C for more than 24 h and employed for the IR measurement over a wavenumber range 400–4,000 cm^{-1} with a resolution of 4 cm^{-1} via accumulation of 32 scans.

Elemental analysis was made with a Yanaco CHN Corder MT series (for C and H quantifications) and a combustion ion chromatography system XS-100 constituted of an ion chromatograph pre-treatment unit AQF-100 (Mitsubishi Chemical Analytech, Co., Ltd.) and an ion chromatograph ICS-1500 (Dionex Corp.) (for F quantification).

Gel permeation chromatography (GPC) was carried out with a Tosoh HLC-8220 GPC apparatus. The measuring conditions were as follows: column, two Tosoh TSK Super HZM-H columns connected with each other; flow rate, 0.25 mL min^{-1} ; temperature, 40 °C; eluent, THF; standard, monodispersed polystyrene.

Differential scanning calorimetry (DSC) analysis was performed on a Seiko DSC 6200/EXSTAR 6000 apparatus. Both the temperature and enthalpy readings were calibrated with an indium standard. The measurements were conducted on ca. 5.5-mg samples, each packed in an aluminum pan, under a nitrogen atmosphere. Each sample was first heated from ambient temperature (~25 °C) to 200 °C at a scanning rate of 15 °C min^{-1} , and then immediately cooled to –90 °C at a rate of 10 °C min^{-1} . Following this, the second heating scan was run from –90 to 200 °C at a rate of 10 °C min^{-1} . The glass transition temperature (T_g) and the mesophase–isotropic phase transition temperature (T_{i-a}) and enthalpy (ΔH_{i-a}) were estimated from thermograms obtained in the second heating scan. The T_g here was taken as a temperature at the midpoint of a baseline shift in heat flow characterizing the glass transition, and the T_{i-a} and ΔH_{i-a} were determined from the peak position and peak area of the relevant endothermic signal appearing in the thermogram.

Polarized optical microscopy (POM) was conducted by using an Olympus microscope BX60F5 equipped with a Mettler FP82HT/FP90 hot stage. Samples (~20 mg) were sandwiched between a slide and cover glass.

Circular dichroism (CD) and optical rotatory dispersion (ORD) spectra were recorded on a Jasco J-820DH spectropolarimeter equipped with a Peltier-type temperature controller PTC-423L. Samples (~15 mg) were sandwiched between two glass plates, to expand into a liquid layer of thickness ~100 μm at the measurement temperature (typically 70 $^{\circ}\text{C}$). Prior to the actual measurement, each sample was allowed to stand for >12 h at the temperature in order to relax possible shear stresses. Refractive index measurements were carried out using an Abbé refractometer (Atago Co., Ltd., Type 2T) equipped with a thermoregulated stage and polarizer rotatable over the eyepiece. For anisotropic samples, the principal refractive indices parallel (n_{\parallel}) and perpendicular (n_{\perp}) to the plane of the prism surfaces were read off. An average refractive index (\tilde{n}) of the mesomorphic medium was evaluated using the formula $\tilde{n} = (2n_{\parallel} + n_{\perp})/3$ in this study.

Wide-angle X-ray diffraction (WAXD) measurements were made on a Rigaku Ultima-IV diffractometer in a reflection mode. Nickel-filtered $\text{CuK}\alpha$ (0.1542 nm) radiation was used at 40 kV and 40 mA. Fluid samples were relaxed for 12 h in a copper sample holder of 0.50 mm height at the prescribed temperature (usually 70 $^{\circ}\text{C}$), and diffraction intensity profiles were collected in the range of $2\theta = 2\text{--}40^{\circ}$. Concerning a sequence of WAXD measurements for a selected sample at different temperatures (30–200 $^{\circ}\text{C}$), each measurement was made after the sample (once annealed) was held at a set temperature for ~35 min. The set temperature was varied by heating at a rate of 10 $^{\circ}\text{C min}^{-1}$.

Results and discussion

Structure determination of Bu7FBu-HPC products

The successful preparation of Bu7FBu-HPC products was confirmed by FT-IR and ^1H NMR measurements and elemental analysis. Figure 1 compiles FT-IR spectra obtained for the ten products and the original HPC. The specific OH stretching band ($3,200\text{--}3,600\text{ cm}^{-1}$) appearing in the HPC spectrum completely vanished after the butyrylation and subsequent heptafluorobutyrylation. Instead, an absorption peak located at $1,736\text{ cm}^{-1}$ and another one at $1,780\text{ cm}^{-1}$, derived from C=O stretching vibrations of the Bu and 7FBu groups, respectively, were observed in the spectra of the Bu7FBu-HPC products; the variation in relative intensity of the two IR signals reflects the proportion of the heptafluorobutyryl (7FBu) to butyryl (Bu) substituents, as supported by elemental analysis data (see Table 2). ^1H NMR spectra of the HPC derivatives are exemplified in Fig. S1 and S2 (see Supporting Information). Besides identification of the products, a possible ester-exchange in the heptafluorobutyrylation of Bu-HPC was found to be essentially negligible.

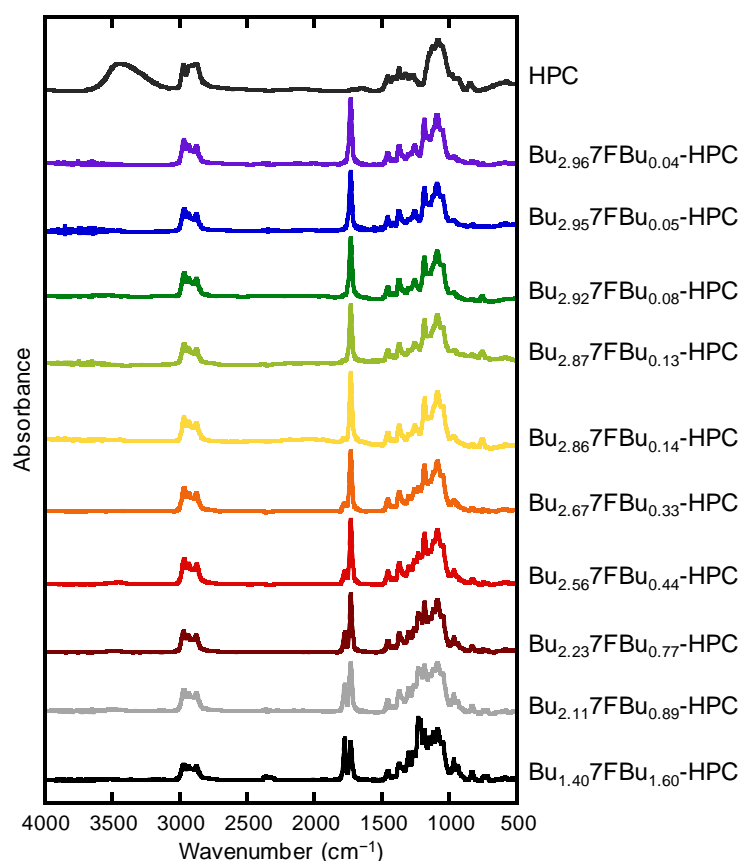


Fig. 1 FT-IR spectra of HPC and Bu7FBu-HPCs

210
211 The structural parameters DS_{Bu} and DS_{7FBu} were calculated on the basis of the result of
212 the elemental analysis and by using a few additional predetermined data. The carbons
213 constituting a Bu7FBu-HPC product include 6 carbons in the AGU, $3 \times MS_{pr}$ carbons in the
214 oxypropylene sequence, $4 \times DS_{Bu}$ carbons in the butyryl side-chain, and $4 \times DS_{7FBu}$ carbons in
215 the heptafluorobutyryl side-chain. The number of fluorine in the product is $7 \times DS_{7FBu}$.
216 Therefore, the following equation holds:

$$217 \quad ([C]/12.01)/([F]/19.00) = (6 + 3 \times MS_{pr} + 4 \times DS_{Bu} + 4 \times DS_{7FBu}) / (7 \times DS_{7FBu}) \quad (1)$$

218 where [C] and [F] are the weight fractions of C and F, respectively, obtained by the elemental
219 analysis. Using a relation, $DS_{Bu} + DS_{7FBu} = 3$, for the full-substituted product (assured by
220 FT-IR measurements) and $MS_{pr} = 4.87$ for the HPC material, we can determine DS_{7FBu} and
221 DS_{Bu} values. Table 2 summarizes the result of the calculations for all the Bu7FBu-HPC
222 products. The DS_{7FBu} values ranged from 0.04 to 1.60.

223 In an alternative method, DS_{Bu} evaluation was first made using a 1H NMR spectrum of
224 each Bu7FBu-HPC, and then DS_{7FBu} was quantified using the DS_{Bu} value and the elemental
225 analysis data (see examples in Supporting Information). The DS_{7FBu} values thus obtained
226 were in good agreement with the corresponding ones given in Table 2, although there
227 occurred a small difference ($< \sim 0.1$) between the two compared DS_{Bu} values.

228
229 **Table 2** Data of wt% element, degree of substitution, and molecular weight for
230 Bu7FBu-HPC products

Sample code	Element (wt%)			DS		Molecular weight		
	H	C	F	DS_{Bu}	DS_{7FBu}	$M_n/10^4$	$M_w/10^4$	M_w/M_n
Bu _{2.96} 7FBu _{0.04} -HPC	8.57	58.94	0.74	2.96	0.04	1.97	6.62	3.36
Bu _{2.95} 7FBu _{0.05} -HPC	8.29	58.77	1.00	2.95	0.05	1.89	7.33	3.89
Bu _{2.92} 7FBu _{0.08} -HPC	8.45	58.29	1.64	2.92	0.08	1.95	7.92	4.06
Bu _{2.87} 7FBu _{0.13} -HPC	8.44	57.56	2.56	2.87	0.13	1.91	7.60	3.99

Bu _{2.86} 7FBu _{0.14} -HPC	8.39	58.17	2.72	2.86	0.14	1.85	7.36	3.98
Bu _{2.67} 7FBu _{0.33} -HPC	7.83	55.83	6.35	2.67	0.33	1.85	7.62	4.13
Bu _{2.56} 7FBu _{0.44} -HPC	7.46	54.29	8.17	2.56	0.44	1.74	7.53	4.32
Bu _{2.23} 7FBu _{0.77} -HPC	6.93	51.68	13.61	2.23	0.77	1.90	8.82	4.65
Bu _{2.11} 7FBu _{0.89} -HPC	6.58	50.37	15.20	2.11	0.89	1.99	7.25	3.64
Bu _{1.40} 7FBu _{1.60} -HPC	5.42	45.62	24.84	1.40	1.60	2.07	9.00	4.34

231

232 Table 2 also compiles data of the molecular weights for the ten Bu7FBu-HPC products.

233 The observed data, $M_n = \sim 19,000$ and $M_w = 66,000\text{--}90,000$, were comparable to $M_n = 2.02 \times$

234 10^4 and $M_w = 7.29 \times 10^4$ of the original HPC, and reasonably it can be assumed that there was

235 no noticeable degradation of the main chain during the acylation reactions.

236 As shown in the Experimental Part, the products listed in Table 2 were all readily soluble

237 in THF, acetone, and chloroform, while being insoluble in water. Using three representative

238 Bu7FBu-HPC samples of $DS_{7FBu} = 0.04, 0.33$, and 1.60 , we further examined the solubility in

239 conventional solvents such as ethanol, *N,N*-dimethylformamide (DMF), and dimethyl

240 sulfoxide (DMSO). The test was made by visual observation at room temperature ($\sim 20^\circ\text{C}$)

241 for each polymer/solvent mixture at a concentration of $1\text{--}1.5\text{ wt\%}$. As a result, the samples

242 of $DS_{7FBu} = 0.04$ and 0.33 dissolved in ethanol and DMF, but the one of $DS_{7FBu} = 1.60$ was

243 insoluble (only swelled) in both the solvents. In the employment of DMSO, none of the

244 samples dissolved in this solvent, although the two sample of $DS_{7FBu} = 0.04$ and 0.33 swelled

245 slightly. Therefore, at least, we can deduce that the solubility of the derivative Bu7FBu-HPC

246 in polar solvents becomes worse as the proportion of the fluoroacyl substitution increases.

247

248 Thermal transition behavior of Bu7FBu-HPCs

249

250 As-prepared products of Bu7FBu-HPC were generally in a highly viscous semi-fluid

251 state at room temperature. Their thermal transition behavior was examined by DSC analysis

and POM observations. Figure 2 illustrates DSC thermograms (part a) and POM

photographs (part b) measured for Bu_{2.87}7FBu_{0.13}-HPC. In the first heating scan of the DSC,

this sample gave an endothermic peak at 164.7 °C, and, in the following cooling scan, it

provided an exothermic peak at 156.4 °C and a large shift in the baseline below −40 °C; this

baseline shift is definitely derived from the glass transition. In the second heating scan, the

sample showed a T_g signal at −44.2 °C (midpoint) and an endothermic peak at 162.9 °C with

the transition enthalpy of $\sim 2.5 \text{ J g}^{-1}$. In the POM observations for the same sample, the field

of view was bright at temperatures lower than 150 °C but became dark in the range of

155–165 °C (see Fig. 2b). From these observations, it is evident that the DSC exo- and

endo-therms signalized a phase transition between an isotropic liquid (I) and an anisotropic

mesophase (M). It should also be noted that, upon cooling, the mesomorphic anisotropy was

frozen into the glassy state (G) of the sample that showed no regular crystallinity. In the

additional cycles of heating and cooling, the Bu₇FBu-HPC product showed the same

enantiotropic phase behavior of $G \leftrightarrow M \leftrightarrow I$.

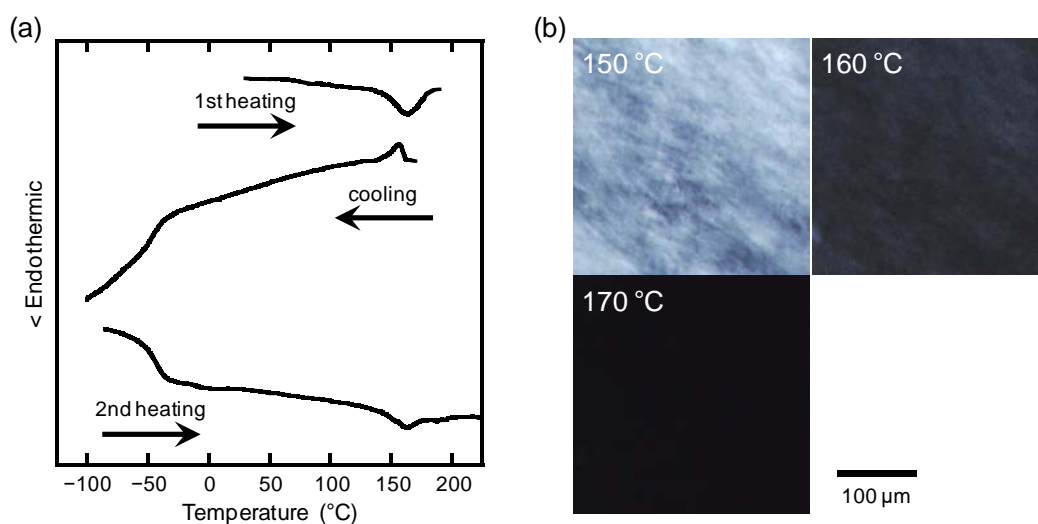


Fig. 2 (a) DSC thermograms and (b) POM images for Bu_{2.87}7FBu_{0.13}-HPC. The POM data

were taken in the second heating process from 10 °C

A similar transition pattern was confirmed for the other Bu7FBu-HPCs. Figure 3 exemplifies DSC thermograms obtained in the second heating scan for all the products, indicating the same transformation of $G \rightarrow M \rightarrow I$. Table 3 summarizes data of the phase transition temperature (T_{i-a}) and enthalpy (ΔH_{i-a}), T_g , and $\Delta T_M (= T_{i-a} - T_g)$ determined from the thermograms. The transition entropy ΔS_{i-a} was calculated from $\Delta S_{i-a} = \Delta H_{i-a}/T_{i-a}$ by assuming an equilibrium at T_{i-a} . As can be seen from the table, T_g and T_{i-a} did not so greatly vary with the proportion of the introduced 7FBu substituent; however, the temperatures were comparatively higher for the Bu7FBu-HPCs of $DS_{7FBu} > 0.44$ and tended to gradually rise with increasing DS_{7FBu} . The DS dependence of ΔH_{i-a} and ΔS_{i-a} was also generally moderate, but the values systematically decreased with increasing DS_{7FBu} when this parameter exceeded 0.4; thus the order of molecular arrangement in the mesophase seems to become slightly lowered with increasing prominence of the dual esterification. An observation worthy of note is that all the Bu7FBu-HPC products were liquid-crystalline in a wide temperature range ($\Delta T_M \geq 200$ °C) of practical use (ca. -30 – 160 °C).

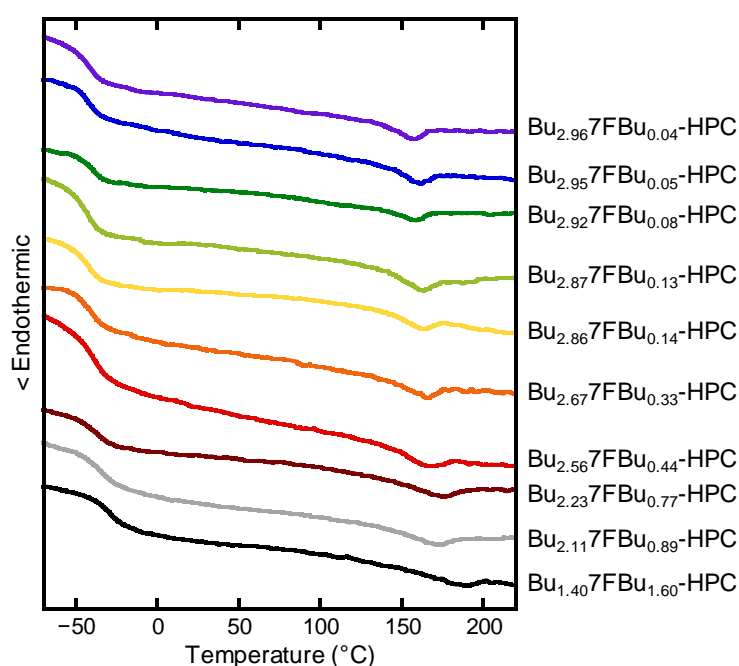


Fig. 3 DSC thermograms of Bu7FBu-HPCs, obtained in the second heating scan

Table 3 Thermal transition temperatures, enthalpy, and entropy of Bu7FBu-HPCs measured by DSC

Sample code	T_g (°C)	T_{i-a} (°C)	ΔT_M (°C)	ΔH_{i-a} (J g ⁻¹)	ΔS_{i-a} (mJ K ⁻¹ g ⁻¹)
Bu _{2.96} 7FBu _{0.04} -HPC	-43.6	158.1	201.7	2.25	5.22
Bu _{2.95} 7FBu _{0.05} -HPC	-41.3	161.8	203.1	2.31	5.31
Bu _{2.92} 7FBu _{0.08} -HPC	-38.9	158.6	197.5	1.59	3.68
Bu _{2.87} 7FBu _{0.13} -HPC	-44.2	162.9	207.1	2.54	5.83
Bu _{2.86} 7FBu _{0.14} -HPC	-43.3	162.7	206.0	1.51	3.46
Bu _{2.67} 7FBu _{0.33} -HPC	-41.3	165.1	206.4	2.22	5.07
Bu _{2.56} 7FBu _{0.44} -HPC	-39.5	168.3	207.8	1.87	4.24
Bu _{2.23} 7FBu _{0.77} -HPC	-38.2	175.3	213.5	1.63	3.63
Bu _{2.11} 7FBu _{0.89} -HPC	-35.0	173.2	208.2	1.25	2.80
Bu _{1.40} 7FBu _{1.60} -HPC	-27.2	190.6	217.8	1.09	2.35

Chiral nematic structure and optical properties of Bu7FBu-HPC thermotropics

DS_{7FBu} dependence

All of the mesophases formed by the Bu7FBu-HPC samples were of chiral nematic type, as proved by the optical evidences shown below.

Figure 4 displays CD spectra measured for a series of Bu7FBu-HPC samples at 70 °C, a temperature intermediate between T_g and T_{i-a} for any sample. The CD peaks observed here signalize the selective light-reflection originating from the supramolecular helical periodicity in the chiral nematic structure. As can be seen in the figure, the position (λ_M) giving a peak maximum shifted systematically to longer wavelengths as the DS_{7FBu} of the used sample increased. Plainly this DS_{7FBu} dependence is quite sharp, differing from that of the thermal

transition behavior (Fig. 3). The reflection spectra of eight samples with various DS_{7FBu} 's ranging from 0.04 to 0.77 covered an entire spectral range from violet to red. This shift in λ_M to the red side was qualitatively confirmed by visual observations of the reflective colors of the thermotropic samples. Two samples of $DS_{7FBu} = 0.89$ and 1.60 were visually colorless and gave no explicit reflection band in the ordinary range (280–880 nm) of the CD measurement.

The specific wavelength λ_M defined above can be related to the chiral nematic pitch P by the de Vries equation (de Vries 1951):

$$\lambda_M = \tilde{n} P \quad (2)$$

where \tilde{n} is an average refractive index of the mesophase. Using data of λ_M and \tilde{n} , P was calculated for the eight Bu7FBu-HPC samples of $DS_{7FBu} = 0.04$ –0.77; roughly, the pitch moved from 280 to 525 nm (see Table S1). Concerning the rotatory sense (handedness) in the chiral nematic structure, it is taken as right-handed for all these thermotropics; this decision is based on the negative sign in ellipticity of the CD peaks.

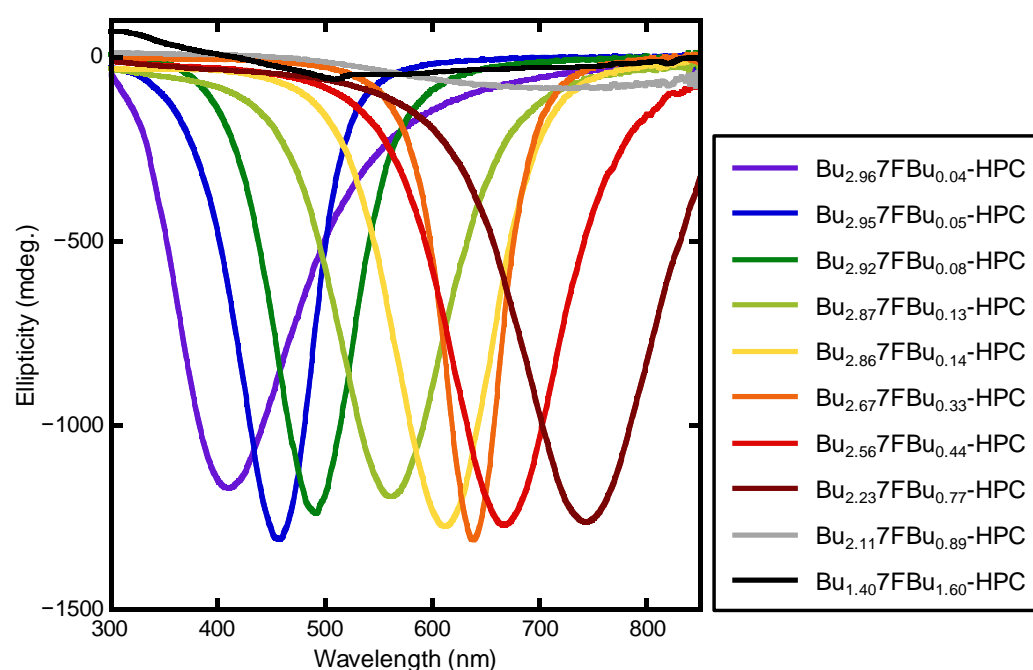


Fig. 4 CD spectra of Bu7FBu-HPCs, measured at 70 °C

With regard to the remaining samples, Bu_{2.11}7FBu_{0.89}-HPC and Bu_{1.40}7FBu_{1.60}-HPC, the pitch and handedness of their mesophases were determined by POM and ORD measurements, respectively. The POM observations revealed that both the mesophases (70 °C) were endowed with a well-developed fingerprint texture characteristic of a chiral nematic liquid crystal with comparatively longer helical periodicity. Figure 5a illustrates the optical image for the mesophase of Bu_{2.11}7FBu_{0.89}-HPC. The repeating distance (S) of the so-called retardation lines making up the texture is, ideally, taken as corresponding to $P/2$. From assessment of the average of S , P of the mesophase of Bu_{2.11}7FBu_{0.89}-HPC was estimated at 5.37 μm . Similarly $P = 11.1 \mu\text{m}$ was evaluated for the other sample Bu_{1.40}7FBu_{1.60}-HPC. In the meantime, these two samples gave an ORD spectrum that obeyed a positive function increasing monotonically with the decrease of wavelength, as shown in Fig. 5b. In general, wavelength dependence of the optical rotation caused by a chiral nematic mesophase is formulated in the following fashion (de Vries 1951; Guo and Gray 1994).

$$\alpha = \pi(\Delta n)^2 P / [4\lambda^2 \{1 - (\lambda/\lambda_M)^2\}] \quad (3)$$

where α is the optical rotation per unit length for light of wavelength λ , λ_M is the wavelength of selective light reflection, Δn is the birefringence of a nematic layer as structural constituent, and the pitch P here is taken to be a pseudoscalar that is positive for a right-handed helix and negative for a left-handed helix. For the case of $\lambda/\lambda_M \ll 1$, Eq. 3 reduces to

$$\alpha \approx \pi(\Delta n)^2 P / 4\lambda^2 \quad (4)$$

Therefore, in the wavelength region of $\lambda \ll \lambda_M$, it follows that α assumes positive or negative values when the chiral nematic phase is right-handed or left-handed, respectively (Guo and Gray 1994). Thus we can deduce that the two samples concerned formed a right-handed chiral nematic arrangement.

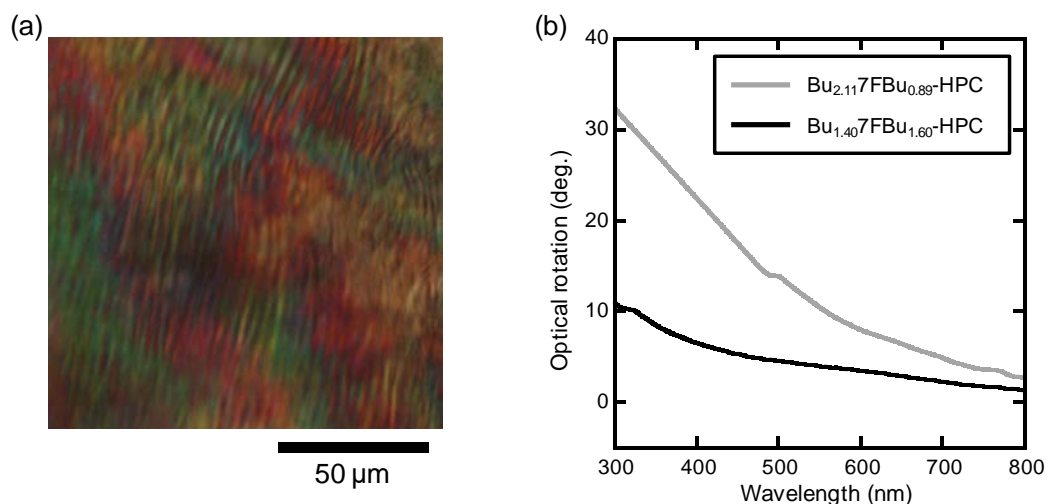


Fig. 5 (a) POM image of Bu_{2.11}7FBu_{0.89}-HPC and (b) ORD spectra of Bu_{2.11}7FBu_{0.89}-HPC and Bu_{1.40}7FBu_{1.60}-HPC. All the data were obtained at 70 °C

The P data of all the Bu7FBu-HPC thermotropics (70 °C) are plotted in Fig. 6 as a function of DS_{7FBu} . Broadly, the P vs. DS_{7FBu} plot seems to make upward curvature. The rise of P at the early stage before DS_{7FBu} reaches ~ 0.3 is particularly steep. There is an abrupt increase of P with the increase of DS_{7FBu} from 0.77 to 0.89. However, attention should be paid to an overestimation of P possible in POM observations; because the helical axis of the chiral nematic structure is not wholly perpendicular to the observation direction.

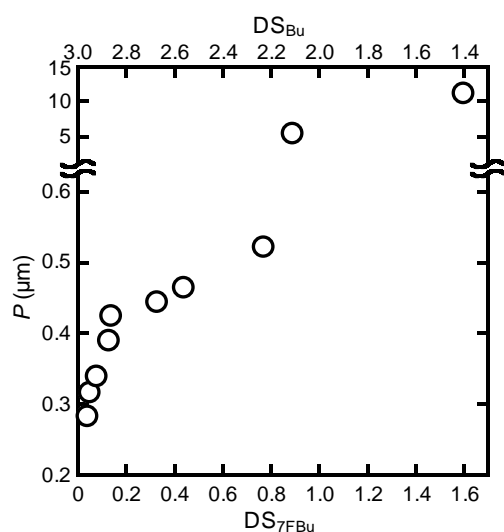


Fig. 6 Chiral nematic pitch P as a function of DS_{7FBu} for a series of Bu7FBu-HPC

thermotropics at 70 °C

Temperature dependence

Figure 7 illustrates CD spectra measured at different temperatures of 20–90 °C for three Bu7FBu-HPCs ($DS_{7FBu} = 0.05, 0.13, \text{ and } 0.77$). Any of the three examples demonstrates a systematic red shift in λ_M of the selective light reflection, with the elevation in temperature. Particularly the Bu_{2.87}7FBu_{0.13}-HPC sample can impart reflective colors covering the whole wavelength region of visible lights in the practical range of temperature. From λ_M data obtained from these CD spectra, the chiral nematic pitch P was calculated by Eq. 2. For the calculation for each sample, the index \tilde{n} at 70 °C (e.g., 1.445 for Bu_{2.87}7FBu_{0.13}-HPC) was adopted, because the temperature variation did not greatly affect the second decimal place of the \tilde{n} data. In Fig. 8, the reciprocal of pitch (P^{-1}) is plotted against temperature for the three Bu7FBu-HPC samples. It is found that P^{-1} decreases almost linearly with elevating temperature and the decreasing rate becomes gradual with increasing in DS_{7FBu} of the derivative.

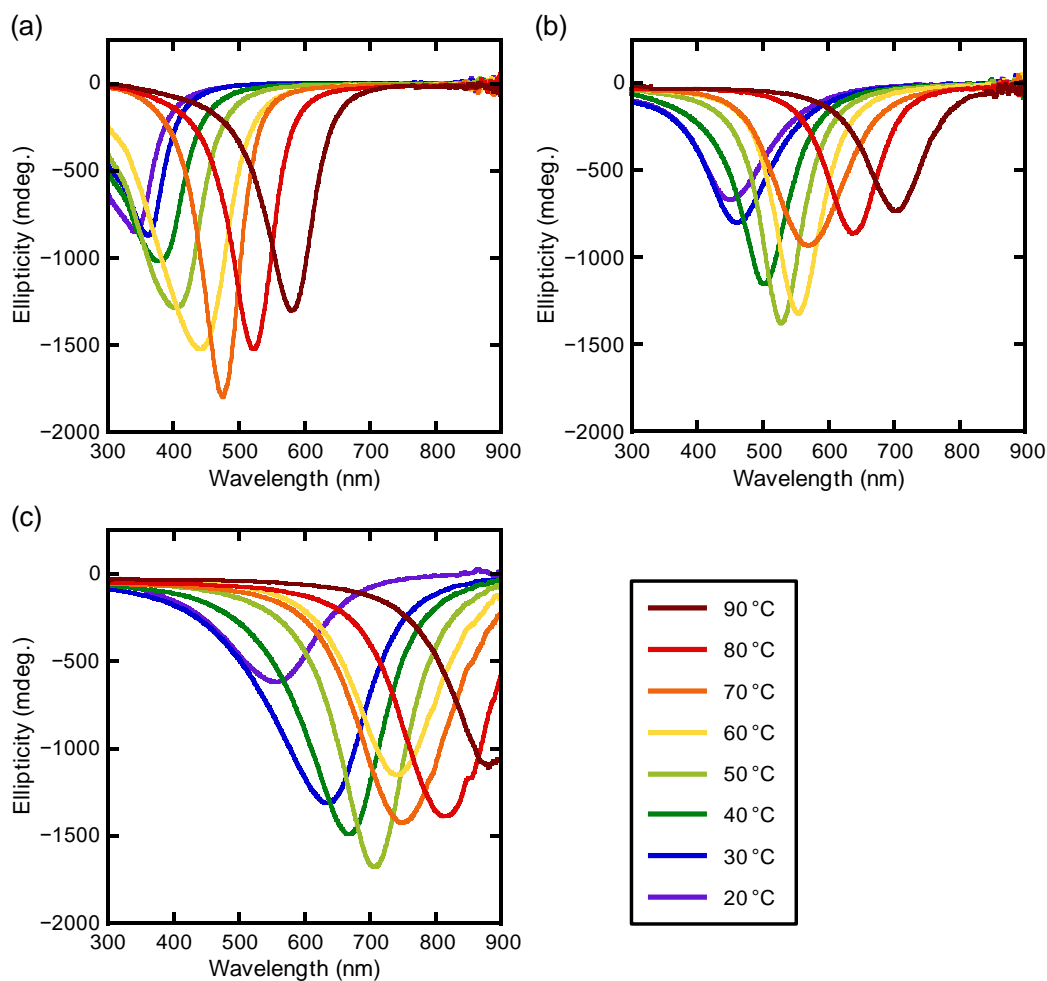


Fig. 7 CD spectra of (a) Bu_{2.95}7FBu_{0.05}-HPC, (b) Bu_{2.87}7FBu_{0.13}-HPC, and (c) Bu_{2.23}7FBu_{0.77}-HPC, measured at temperatures ranging from 20 to 90 °C

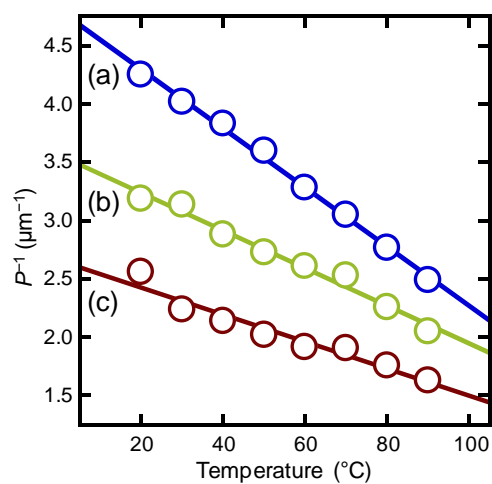


Fig. 8 P^{-1} versus temperature plots for (a) Bu_{2.95}7FBu_{0.05}-HPC, (b) Bu_{2.87}7FBu_{0.13}-HPC, and (c) Bu_{2.23}7FBu_{0.77}-HPC

384

385 A similar linearity of P^{-1} versus temperature (T) has been observed for other
386 thermotropic HPC derivatives (Kosho et al. 1999; Laivins and Gray 1985; Ritcey and Gray
387 1988), typically expressed in the following empirical form:

$$388 \quad P^{-1} = a(1 - T/T_n) \quad (5)$$

389 where a is a constant and T_n is a temperature at which the nematic state of $P = \infty$ is attained.
390 According to this relation, when T is elevated to exceed T_n , the handedness of the chiral
391 nematic arrangement should be reversed, for instance, from right ($P > 0$) to left ($P < 0$) in the
392 present thermotropics of Bu7FBu-HPC. In view of this, we extrapolated the linear plots
393 shown in Fig. 8 and estimated the specific temperature T_n to be 195, 220, and 229 °C for
394 Bu_{2.95}7FBu_{0.05}-HPC, Bu_{2.87}7FBu_{0.13}-HPC, and Bu_{2.23}7FBu_{0.77}-HPC, respectively. These T_n
395 values exceed the T_{i-a} 's (see Table 3) determined by DSC for these samples. In actuality,
396 therefore, the thermotropic samples solely showed a transition from the right-handed chiral
397 nematic phase to isotropic melt around 155–170 °C, without taking such a handedness
398 inversion.

399

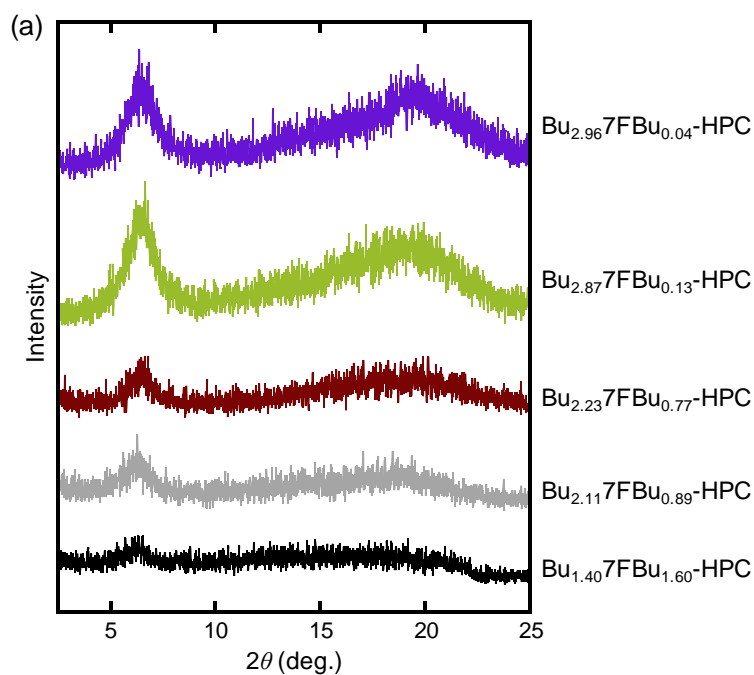
400 Insight into short-range order in mesophases of Bu7FBu-HPC

401

402 Figure 9a illustrates WAXD intensity profiles measured for selected Bu7FBu-HPC
403 thermotropics at 70 °C. All diffraction intensity curves gave only one significant peak at a
404 lower angular position of $2\theta \approx 6.4^\circ$, except for a diffuse scattering halo centered at $2\theta \approx 19^\circ$.
405 Therefore, the Bu7FBu-HPC thermotropics are found to assume an essentially nematic
406 structure, and the short-range order of less than a few nanometers in the mesophase is
407 analyzable in terms of a pseudo-hexagonal packing of the molecular main chains. The
408 distance (d) between the nematic layers stacking in the mesophase can be directly estimated
409 from the low-angle peak by Bragg's equation ($\lambda = 2d\sin\theta$, $\lambda = 0.1542$ nm). Then, the twist

angle (φ), defined as an azimuth difference between adjacent nematic thin layers, is calculated from the relation $\varphi = 360^\circ \times d/P$ by use of the chiral nematic pitch data obtained in optical measurements.

Figure 10a collects d and φ values obtained for the explored ten Bu7FBu-HPC samples (70 °C), by plotting the data as a function of DS_{7FBu} . The distance d was hardly affected by DS_{7FBu} and almost constant at 1.38 nm. In contrast, the twist angle φ sharply decreased with increasing DS_{7FBu} from 1.76° ($DS_{7FBu} = 0.04$) to $\sim 0.1^\circ$ ($DS_{7FBu} = 0.89$). Thus the distinctive variation of P with DS_{7FBu} shown in Fig. 6 is attributable to the variation of φ .



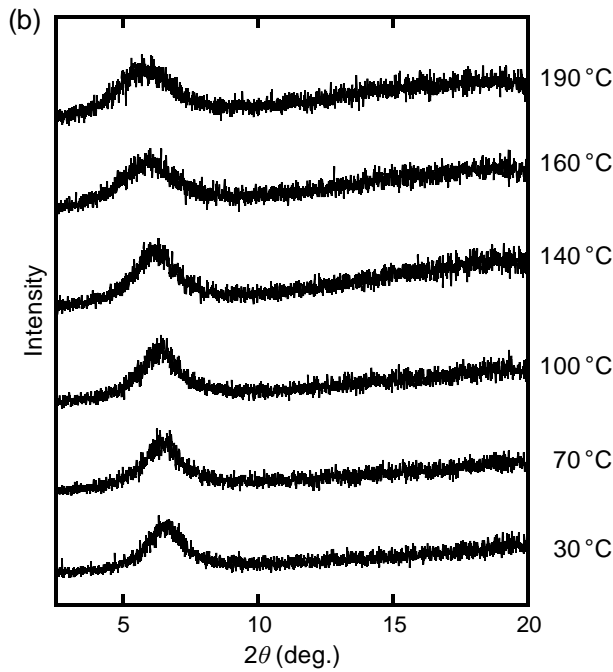


Fig. 9 WAXD intensity profiles obtained for (a) selected Bu7FBu-HPC samples at 70 °C and (b) Bu_{2.877}FBu_{0.13}-HPC at different temperatures

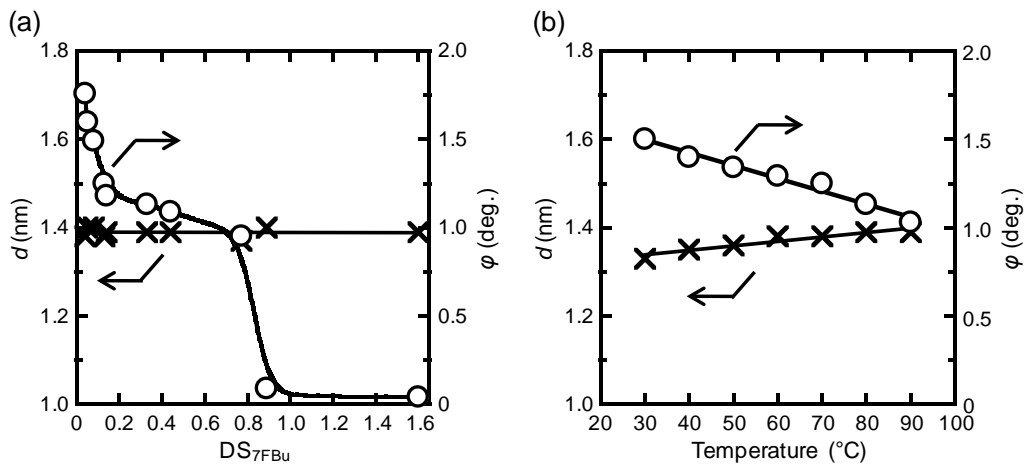


Fig. 10 Plots of the interlayer distance d (cross symbol) and twist angle ϕ (open circle): (a) as a function of DS_{7FBu} of Bu7FBu-HPC; (b) as a function of temperature for Bu_{2.877}FBu_{0.13}-HPC

Figure 9b illustrates temperature dependence of the WAXD profile in the range of $2\theta \leq 20^\circ$ for a representative sample of $DS_{7FBu} = 0.13$, Bu_{2.877}FBu_{0.13}-HPC. The maximum

position of the low-angle peak was situated at $2\theta \approx 6.55\text{--}6.35^\circ$ at temperatures of $30\text{--}130^\circ\text{C}$. Above 140°C , however, the peak became broader and the maximum position shifted explicitly to lower angles ($2\theta < 6^\circ$ at $T > 150^\circ\text{C}$). Plainly this change can be ascribed to the mesophase to isotropic phase transition which was observed at $150\text{--}170^\circ\text{C}$ for this sample ($T_{i-a} = 162.9^\circ\text{C}$, see Fig. 2a). Somewhat surprisingly, as exemplified in Fig. 9b, the short-range hexagonal structure was still retained even at 190°C to some degree in the optically isotropic melt; probably the high viscosity would prevent a rapid decline of the structure.

Figure 10b shows a result of the d and ϕ quantifications as a function of temperature for the $\text{Bu}_{2.87}\text{FBu}_{0.13}\text{-HPC}$ sample; the data plotting was made in the range of $30\text{--}90^\circ\text{C}$ where the pitch P of the mesophase was determinable by CD measurements (Fig. 7b). With the increase in temperature from 30 to 90°C , the d value slightly fluctuated from 1.33 to 1.39 nm , whereas the twist angle ϕ diminished more sensitively from 1.50° to 1.03° . It can therefore be deduced that the increase of P (i.e., the decrease of P^{-1}) with temperature was determined mainly by the variable twist angle.

Finally, we add a remark about the effect of the heptafluorobutyryl group; i.e., why did the introduction of such a fluoroacyl group to the HPC ester result in the sharp decrease in ϕ and ensuing increase in P of the formed chiral nematic mesophase? As is generally known, fluoropolymers having a perfluoroalkyl side chain show unique properties represented by the water- and oil-repellency, low dielectric permittivity, low refractive index, etc. (Hasegawa 2017). The perfluoroalkyl (R_f) chains take an attitude of spontaneous aggregation induced by the dipole-dipole interaction, and the above-mentioned bulk properties of fluoropolymers seem to be dominated strongly by the intrinsic interaction between the R_f groups (Hasegawa 2015, 2017). By deduction, the 7FBu groups of the cellulose derivative Bu7FBu-HPC would also show such a habit of attractive interaction that becomes noticeable in frequency when the $\text{DS}_{7\text{FBu}}$ is increased. Then, the cellulosic main chains constituting a chiral nematic

layer would become arranged to be more parallel to those in the neighboring layers, i.e., the twist angle φ approaches zero, via the increasing 7FBu-attractions between adjacent two layers. This is still a speculative explanation, however.

Conclusions

We successfully prepared a series of fully esterified HPC derivatives, Bu7FBu-HPCs, with various ratios of butyryl (Bu)/heptafluorobutyryl (7FBu) substitutions, $DS_{Bu}/DS_{7FBu} = 2.96:0.04$ – $1.40:1.60$, and investigated the thermotropic phase behavior.

The Bu7FBu-HPC samples formed a chiral nematic mesophase in a wide temperature range between the T_g (≈ -40 – -30 °C) and T_{i-a} (≈ 160 – 190 °C); the transition temperatures elevated gently as the DS_{7FBu} increased. In contrast to the small diversity in thermal transition behavior between the samples, the mesomorphic property derived from the chiral nematic periodicity was much affected by the varying 7FBu proportion. It was proved that the pitch P of the mesophase sharply increased with increasing DS_{7FBu} at a constant temperature, differing from the previous inference (Guittard et al. 1994; Yamagishi et al. 1994). With a constant DS_{7FBu} , the P increased with elevating temperature, in accordance with the general tendency observed for thermotropic HPC esters (Kosho et al. 1999; Yamagishi et al. 1994). The supramolecular helical arrangement remained right-handed and conversion of the handedness was not observed in the present sampling and surrounding conditions. The increases of P responding to the increases in DS_{7FBu} and temperature were attributed to the decrease of the twist angle between adjacent nematic layers. This angular decrease might be related to a possible dipolar interaction between the 7FBu side groups distributed in the space between the layers.

483

484 **Acknowledgments** This work was financed by Grant-in-Aids (KAKENHI) for Scientific
485 Research (A) (No. 26252025 to YN) and Young Scientist Research (B) (No. 17K15295 to KS)
486 from the Japan Society for the Promotion of Science (JSPS).

487

488 **Compliance with ethical standards**

489 **Conflict of interest** The authors declare no conflict of interest.

490

491

492 **References**

493

494 de Vries H (1951) Rotatory power and other optical properties of certain liquid crystals. *Acta*
495 *Crystallogr* 4:219–226

496 Fukuda T, Takada A, Miyamoto T (1994) Thermotropic Cellulose Derivatives. In: Gilbert RD
497 (ed) *Cellulosic Polymers, Blends and Composites*. Hanser, Munich/New York, Chapter 3
498 (pp 47–70)

499 Fukuda T, Tsujii Y, Miyamoto T (1995) Structural characteristics of polysaccharide-based
500 thermotropic liquid crystals. *Macromol Symp* 99:257–267

501 Gilbert RD, Patton PA (1983) Liquid crystal formation in cellulose and cellulose derivatives.
502 *Prog Polym Sci* 9:115–131

503 Gray DG (1983) Liquid crystalline cellulose derivatives. *J Appl Polym Sci Appl Polym Symp*
504 37:179–192

505 Gray DG (1985) Chemical characteristics of cellulosic liquid crystals. *Faraday Discuss Chem*
506 *Soc* 79:257–264

507 Gray DG (1994) Chiral nematic ordering of polysaccharides. *Carbohydr Polym* 25:277–284

508 Gray DG, Harkness BR (1994) Chiral Nematic Mesophases of Lyotropic and Thermotropic

- 509 Cellulose Derivatives. In: Shibaev VP, Lam L (eds) Liquid Crystalline and Mesomorphic
510 Polymers. Springer, New York, pp 298–323
- 511 Guittard F, Yamagishi T, Cambon A, Sixou P (1994) Preparation and liquid crystalline
512 properties of (hydroxypropyl)cellulose perfluorooctanoate. *Macromolecules* 27:6988–6990
- 513 Guo J-X, Gray DG (1994) Lyotropic Cellulosic Liquid Crystals. In: Gilbert RD (ed)
514 Cellulosic Polymers, Blends and Composites. Hanser, Munich/New York, Chapter 2 (pp
515 25–45)
- 516 Hasegawa T (2015) Understanding of the intrinsic difference between normal- and
517 perfluoro-alkyl compounds toward total understanding of material properties. *Chem Phys*
518 *Lett* 627:64–66
- 519 Hasegawa T (2017) Physicochemical nature of perfluoroalkyl compounds induced by fluorine.
520 *Chem Rec* 17:903–917
- 521 Ho FF-L, Kohler RR, Ward GA (1972) Determination of molar substitution and degree of
522 substitution of hydroxypropyl cellulose by nuclear magnetic resonance spectroscopy. *Anal*
523 *Chem* 44:178–181
- 524 Hou H, Reuning A, Wendorff JH, Greiner A (2000) Tuning of the pitch height of thermotropic
525 cellulose esters. *Macromol Chem Phys* 201:2050–2054
- 526 Huang B, Ge JJ, Li Y, Hou H (2007) Aliphatic acid esters of (2-hydroxypropyl)
527 cellulose—Effect of side chain length on properties of cholesteric liquid crystals. *Polymer*
528 48:264–269
- 529 Ishizaki T, Uemura S, Furumi S (2015) Thermotropic properties of cholesteric liquid crystal
530 from hydroxypropyl cellulose mixed esters. *Kobunshi Ronbunshu* 72:737–745
- 531 Kosho H, Hiramatsu S, Nishi T, Tanaka Y, Kawaguchi S, Watanabe J (1999) Thermotropic
532 cholesteric liquid crystals in ester derivatives of hydroxypropylcellulose. *High Perform*
533 *Polym* 11:41–48
- 534 Laivins GV, Gray DG (1985) Optical properties of (acetoxypentyl)cellulose: factors

- 535 influencing the cholesteric pitch. *Polymer* 26:1435–1442
- 536 Lee D, Perlin AS (1982) ^{13}C -N.M.R.-spectral of substituents and related studies on the
537 distribution in *O*-(2-hydroxypropyl)cellulose. *Carbohydr Res* 106:1–19
- 538 Nishio Y (2006) Material functionalization of cellulose and related polysaccharides via
539 diverse microcompositions. *Adv Polym Sci* 205:97–151
- 540 Nishio Y, Sato J, Sugimura K (2016) Liquid crystals of cellulose: fascinating ordered
541 structures for the design of functional material systems. *Adv Polym Sci* 271:241–286
- 542 Ohlendorf P, Greiner A (2015) Synthesis of liquid crystalline thioether-functionalized
543 hydroxypropyl cellulose esters. *Polym Chem* 6:2734–2739
- 544 Ritcey AM, Gray DG (1988) Circular reflectivity from the cholesteric liquid crystalline phase
545 of (2-ethoxypropyl)cellulose. *Macromolecules* 21:1251–1255
- 546 Tseng S-L, Valente A, Gray DG (1981) Cholesteric liquid crystalline phases based on
547 (acetoxypentyl)cellulose. *Macromolecules* 14:715–719
- 548 Werbowyj RS, Gray DG (1976) Liquid crystalline structure in aqueous hydroxypropyl
549 cellulose solutions. *Mol Cryst Liq Cryst (Lett)* 34:97–103
- 550 Werbowyj RS, Gray DG (1980) Ordered phase formation in concentrated hydroxypropyl
551 cellulose solutions. *Macromolecules* 13:69–73
- 552 Yamagishi T, Guittard F, Godinho MH, Martins AF, Cambon A, Sixou P (1994) Comparison
553 of thermal and cholesteric mesophase properties among the three kind of
554 hydroxypropylcellulose (HPC) derivatives. *Polym Bull* 32:47–54
- 555 Yamagishi T, Nakamoto Y, Sixou P (2006) Preparation and cholesteric mesophase properties
556 of (butyl-*co*-pentyl) propylcellulose. *Cellulose* 13:205–211
- 557 Zugenmaier P (1994) Polymer Solvent Interaction in Lyotropic Liquid Crystalline Cellulose
558 Derivative Systems. In: Gilbert RD (ed) *Cellulosic Polymers, Blends and Composites*.
559 Hanser, Munich/New York, Chapter 4 (pp 71–94)
- 560 Zugenmaier P (1998) Cellulosic Liquid Crystals. In: Demus D, Goodby J, Gray GW, Spiess

561 H-W, Vill V (eds) Handbook of Liquid Crystals, Vol 3. Wiley-VCH, Weinheim, Chapter IX
562 (pp 453–482)

563

564

565 -----

566

567 **Electronic supplementary material** The online version of this article
568 (<https://doi.org/10.1007/s10570-018-2176-6>) contains supplementary material, which is
569 available to authorized users.

570